COMPDYN 2015
5th ECCOMAS Thematic Conference on
Computational Methods in Structural Dynamics and Earthquake Engineering
M. Papadrakakis, V. Papadopoulos, V. Plevris (eds.)
Crete Island, Greece, 25–27 May 2015

A NOVEL MECHANISM FOR RESTRAINING SEISMIC ACTIONS IN DUCTILE BRIDGES: ANALYTICAL MODELING AND EXPERIMENTAL VERIFICATION

Vasileios G. Pilitsis, Vassilis K. Papanikolaou, Ioannis A. Tegos and Kosmas-Athanasios Stylianidis

Aristotle University of Thessaloniki
Faculty of Engineering
School of Civil Engineering
Laboratory of Reinforced Concrete and Masonry
vpilitsi@civil.auth.gr
billy@civil.auth.gr
itegos@civil.auth.gr
kcstyl@civil.auth.gr

Keywords: Integral bridges, abutment, serviceability, experimental, seismic.

Abstract. *In the present study, a mechanism for restraining seismic actions on ductile bridges is suggested and verified analytically and experimentally. The mechanism consists of the wall abutment which is monolithically connected to the end of the deck and is rested either on elastomeric bearings on the pile cap or on the abutment foundation as a stopper of adequate width, based on the serviceability demands due to the deck length variation. Using the suggested mechanism, the restraining of seismic deformations is attained on both bridge directions, without any complications during serviceability states, also alleviating stresses in the end-spans due to a more favorable moment distribution. There are Code provisions which permit the computational analytical modeling of the system, however it was considered appropriate to further examine of the proposed mechanism experimentally. For this purpose, eight 1:3 scale specimens of the suggested mechanism were prepared. Four of them were designed for normal (large) shear ratios, while the other four were designed for small shear ratios. The specimens were subjected in cyclic loading and interesting results were observed regarding the three response indexes, namely, strength, stiffness and ductility.*

1 INTRODUCTION

Integral abutment and integral pier bridges are jointless bridge structures whose deck is rigidly connected to the abutment and piers. They improve aesthetics and earthquake resistance compared to traditional systems with expansion joints, bearings and other structural releases which permit expansion/contraction due to thermal actions, creep and shrinkage. The design of bridges has to accommodate both serviceability and earthquake resistance, which are conflicting components of the same problem and they impose opposite design requirements [1].

A novel mechanism for restraining seismic actions in ductile bridges while accommodating serviceability demands has been already suggested as an adjustment on the abutments [2], [3], [4]. The wall-web of the conventional abutment is suggested to be rigidly connected to the end-parts of the deck and the sliding bearings of the abutment are placed on the footing of the abutment wall, which is contained inside a gap (Fig. 1). The gap width depends on the total length of the bridge and is relevant to the expansion/contraction of the deck due to thermal actions and creep/shrinkage. The longitudinal restraining of the approach embankment is secured by the existence of a second wall and its lateral restraining by the wing-walls.

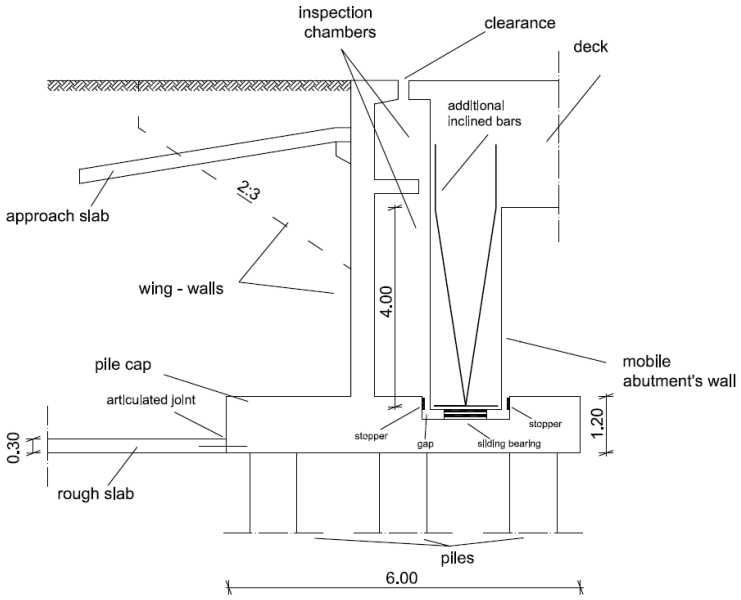

Figure 1: Longitudinal section cut of the novel mechanism.

An experimental investigation of the mechanical behavior of this novel mechanism for restraining seismic actions in ductile bridges is attempted in this study. In particular three response indexes are examined, namely strength, stiffness and ductility. Furthermore, the influence of the gap is examined in terms of energy dissipation capacity and durability of the abutment walls during cyclic loading.

2 SPECIMEN GEOMETRY

Eight cantilever specimens were prepared in 1:3 scale corresponding to the dimensions of two typical cases of wall-web for the suggested type of abutment: (a) a flexible wall-web with a height of 4.50 m and a thickness of 50 cm and (b) a stiffer wall-web with a height of 1.50 m and a thickness of 50 cm. Since it is difficult to achieve full fixity conditions in the laboratory, the eight cantilever specimens were formed as four beams, simply supported in both ends. Two of the beams had a length of 3.20 m while the other two of 1.20 m. Each beam consists

of two cantilevers of net length of 0.375 m for case (a) and 1.375 m for the case (b) (Fig. 2, Fig. 3). The width of the beams was equal to 36 cm for proper mounting of the loading device (actuator) to the beams. In the midspan of each beam, a stiff zone was formed with a thickness of 35 cm and a length of 25 cm, in which the external load is imposed and by which full fixity of each cantilever is achieved. The diagrams of internal forces and the deformed shape of a simply supported beam with a concentrated force in the midspan is equivalent to the composition of two mirrored cantilevers with a concentrated load at one end part, equal to the half of the simply supported beam force (Fig. 4). The hinge supports were placed at 10 cm from the edges of each beam.

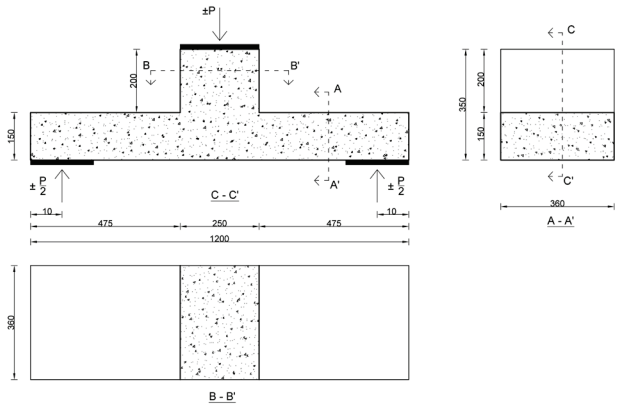

Figure 2: Geometry of the short span specimens.

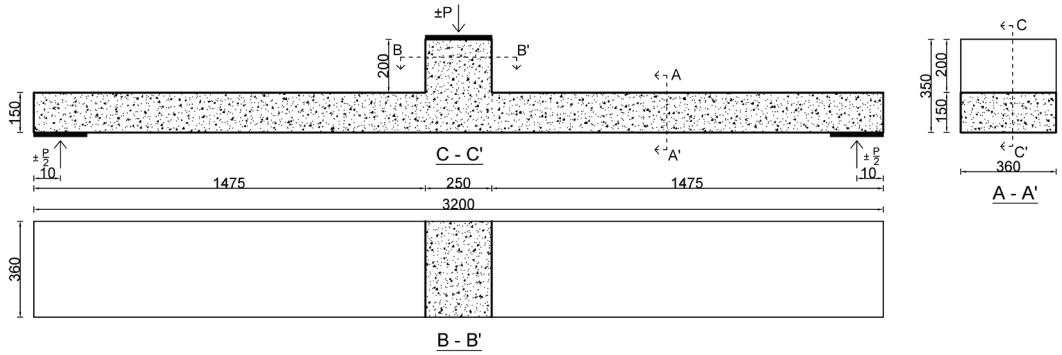

Figure 3: Geometry of the long span specimens.

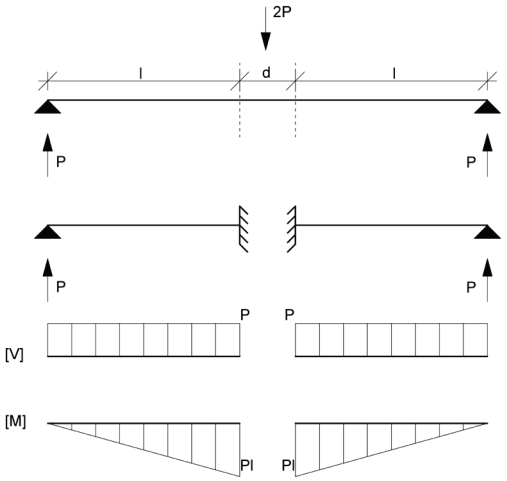

Figure 4: Static system, shear and moment diagrams of the specimens.

3 REINFORCEMENT DETAILING AND MATERIAL PROPERTIES

The longitudinal reinforcement of each specimen consists of ten Ø10 bars, arranged as shown in Fig. 5 and Fig. 6. This corresponds to a longitudinal reinforcement ratio of ρ_l = 1.45 %. The transverse reinforcement selected in both types of specimens guarantee that the specimens will experience flexural failure. The concrete cover was equal to 1.0 cm in both cases.

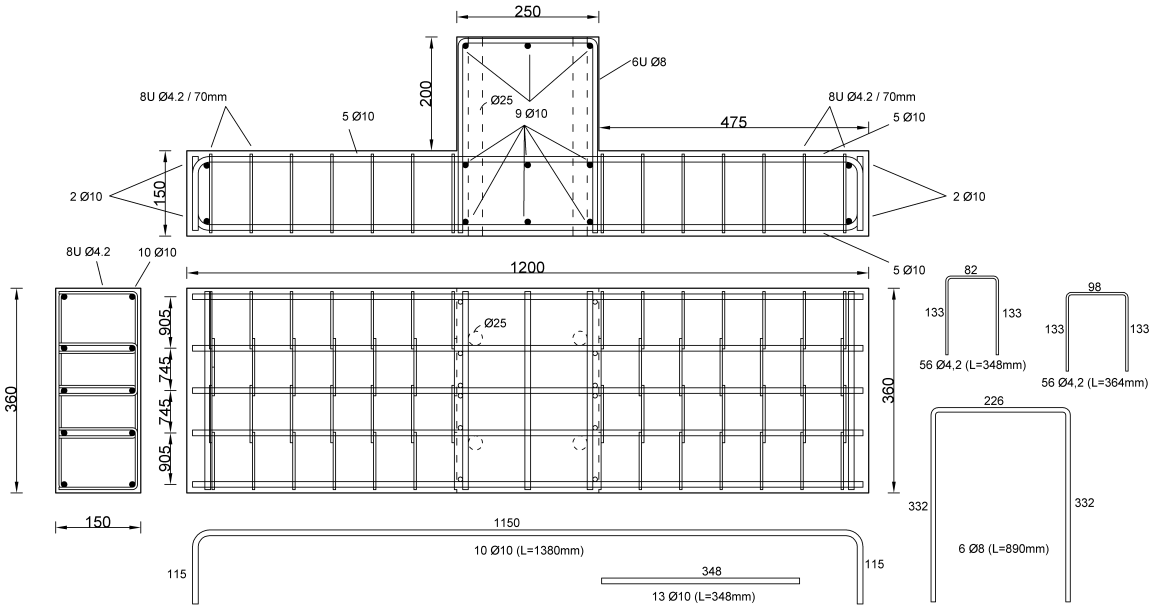

Figure 5: Reinforcement of the short span specimens.

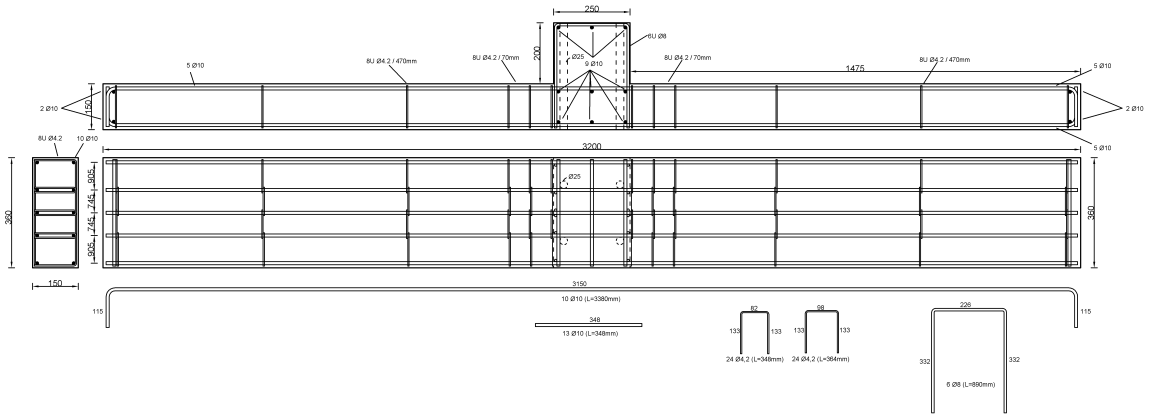

Figure 6: Reinforcement of the long span specimens.

The steel class used for longitudinal reinforcement corresponds to B500A [5]. Yield strength was equal to 586 MPa, the maximum strength equal to 700 MPa, the strain at yielding was ε_y = 2.94 ‰ and the ultimate strain is equal to ε_u = 3.41 %. These values were the mean values of ten specimens of steel rebar used for the longitudinal reinforcement. Similarly, the yield strength of the transverse reinforcement was measured equal to 680 MPa.

The properties of the used concrete were estimated by testing three cubic concrete specimens in uniaxial compression for the case of the short beams (low shear span ratio) and six cubic concrete specimens in the case of the two long beams (high shear span ratio). The

strength class of concrete in the first case was estimated as C25/30 and in the second case as C30/37.

Four through holes with a diameter of 25 mm were formed during casting of the specimens using PVC pipes. The mounting of the loading device (actuator) was achieved by using threaded rods passing through the holes.

The hinge supports at the beam ends were implemented by two steel supports as shown in Fig. 7. The cylindrical rod of each support was inserted in the laboratory floor slab holes (77 mm diameter). The rectangular opening of the steel supports where the beams (15 cm width) are inserted was equal to 16 cm. One short beam and one long beam were firmly mounted in the steel supports steel plates in order to suppress the 1 cm gap, while the other two beams were placed in the opening without closing the gap (i.e. free movement). However, by examining the resulting hysteresis loops of the specimens, the first two beams were not totally fixed in the supports, but a ±2 mm lash was measured. The other two beams had a measured lash of ±3.5 mm (instead of the nominal ±5 mm). The above information is summarized in Table 1.

	Span Length (m)	Concrete Class	Gap Width (mm)
S-4	1.0	C30/37	4
S-7	1.0	C30/37	7
L-4	3.0	C25/30	4
L-7	3.0	C25/30	7

Table 1: Specimen labeling and characteristics.

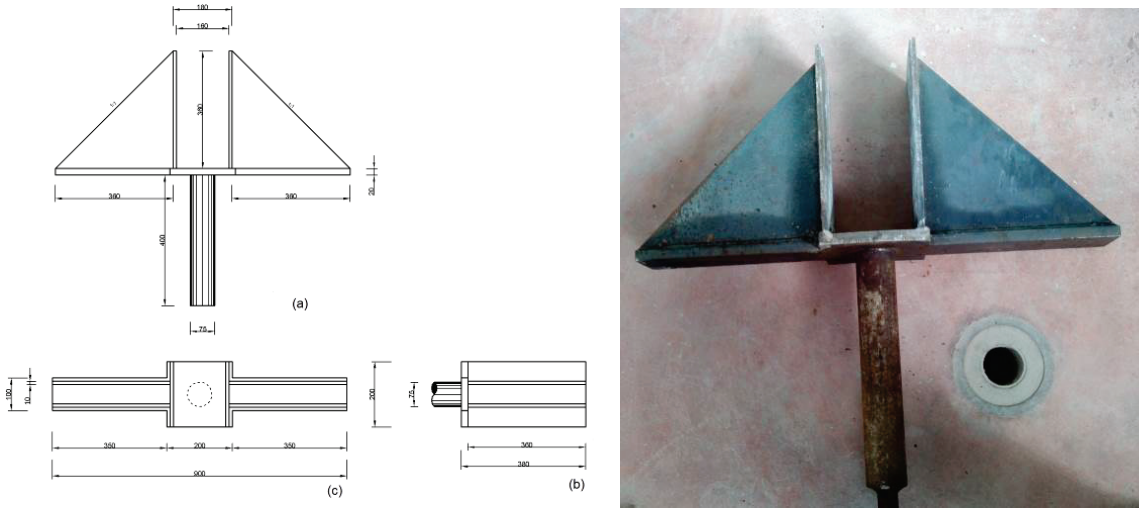

Figure 7: (left) Plans of the steel supports, (right) steel support.

4 EXPERIMENTAL SETUP

The four beams were subjected to cyclic displacement using a hydraulic actuator [6]. The time-history of the imposed displacements for specimens S-4 and S-7 is shown in Fig. 8 (left) and in Fig. 8 (right) for specimens L-4 and L-7. Each time-history is consisted of eighteen cycles divided into groups of three, of equal maximum displacement. Each cycle has duration of two minutes and the total running time is 36 mins.

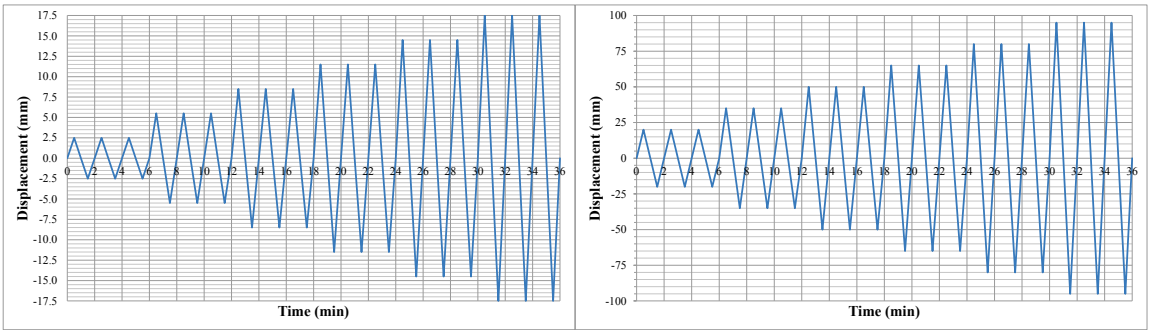

Figure 8: Imposed displacement time-histories of S-4 and S-7 (left) and of L-4 and L-7 (right).

In Fig. 9 a sketch of the experimental setup is shown, for the case of short beams. The cyclic displacement is imposed in the midspan of the beams, where the hydraulic actuator is attached to the rigid zone of the beams through a QHS 140x140x4 mm steel hollow beam of 460 mm length.

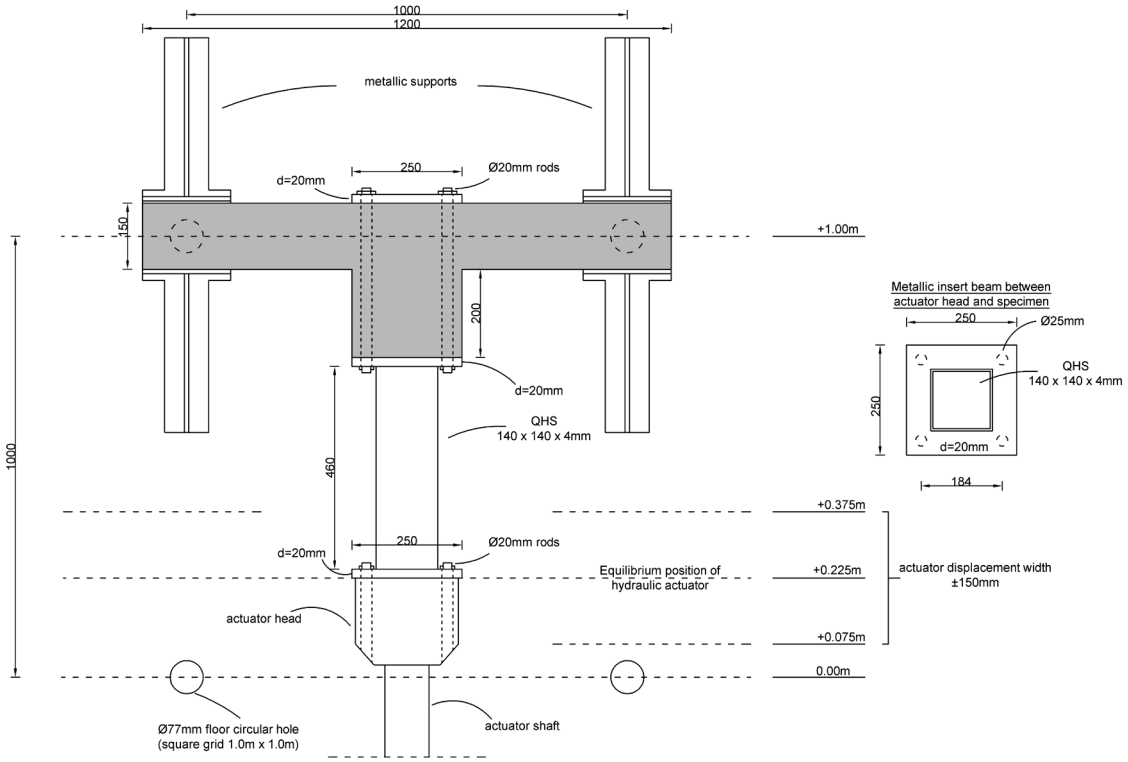

Figure 9: S-specimens position relative to the hydraulic actuator.

The displacement load history was imposed by a double acting hydraulic actuator in the Laboratory of Reinforced Concrete and Masonry Structures, Department of Civil Engineering, Aristotle University of Thessaloniki. Its load capacity is ±250 kN and its full stroke is ±150 mm. The actuator is equipped with a build-in LVDT device for measuring the imposed displacements. However, as shown in Fig. 10, the actuator was mounted on a horizontal support steel beam which is naturally susceptible to (elastic) bending during specimen loading. As a result, additional displacements due to this bending could be picked up by the actuator internal LVDT, resulting to considerable differences between the desired (target) displacement load history and the measured displacement of the internal LVDT. For this reason, the actuator closed-loop control was not based on this internal LVDT (default setting) but was rather

transferred to an external measurement system, specifically an external ±75 mm LVDT for the short beams and a ±112.5 mm draw wire sensor for the long beams, attached to the specimen midspan. This decision was eventually justified by the comparative results shown in Fig. 11, where the blue line shows the actuator internal LVDT measurement for the ±5.5 mm cycle, unfavorably deviating for about 2.5 mm from this target value. On the contrary, the closed-loop reference external LVDT yields the desired target displacement (red line), while the green line shows the support beam midspan displacement (maximum 2 mm, measured using an auxiliary LVDT). The remaining 0.5 mm difference between the internal and external LVDTs can be attributed to mechanical lash of the various mounting bolts.

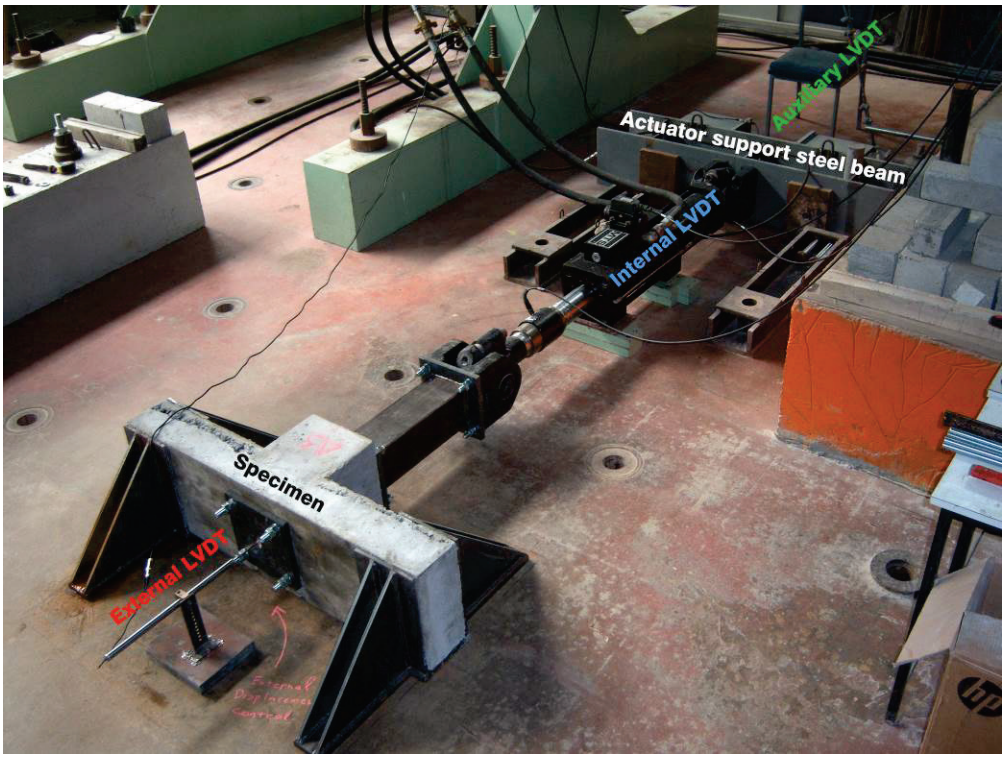

Figure 10: Experimental setup - measurement points.

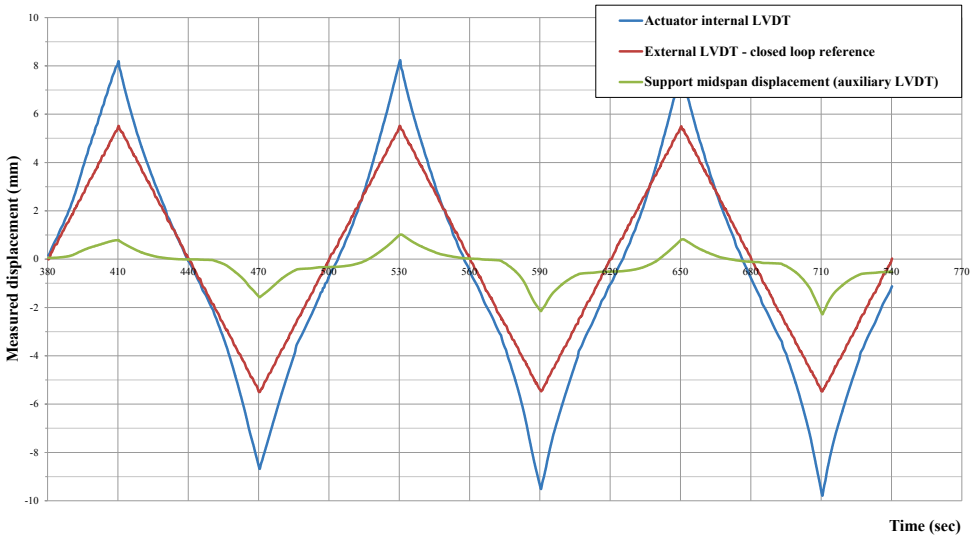

Figure 11: Measurement comparison between internal (actuator) and external closed-loop reference LVDTs.

5 ANALYTICAL CALCULATION OF THE SPECIMEN PROPERTIES

The analytical calculation of the specimen properties regarding deformation and strength is based on Fig. 4 and the results of the section analysis (Fig. 13). These analyses were performed using AnySection v.4.0.4 software [7]. The stress-strain law considered for the concrete behavior was the parabolic-rectangular diagram of EC2-Part 1 [5]. Regarding reinforcement steel, its stress-strain law was initially considered as bilinear without hardening. The analytical results did not approximate well the experimental results and thus a stress-strain diagram according to Park & Sampson [8] was considered, which offered a better approximation (Fig. 12).

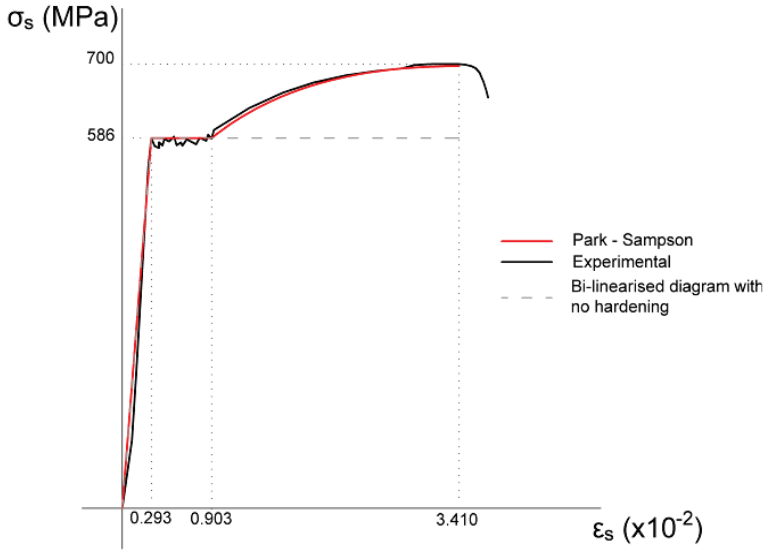

Figure 12: Stress-deformation diagramm of longitudinal reinforcement steel.

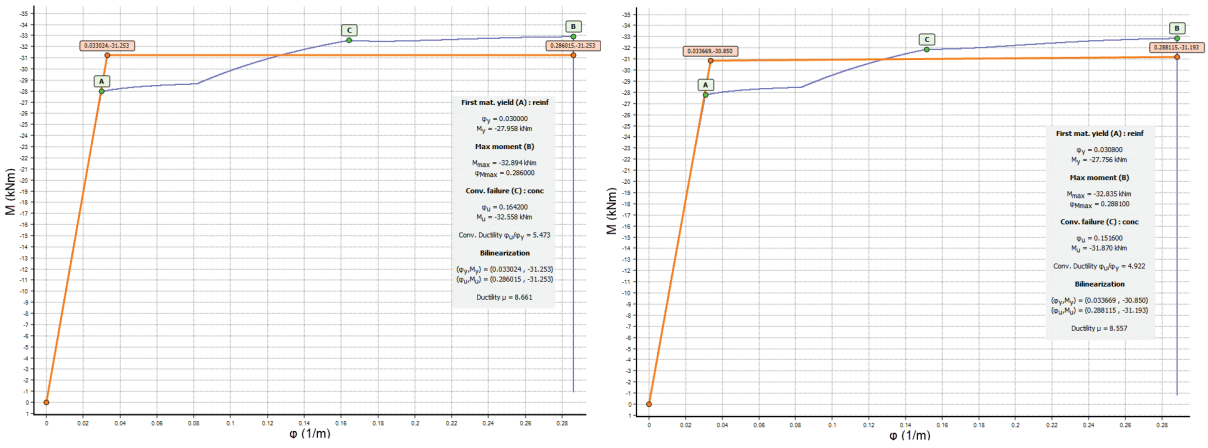

Figure 13: Moment-curvature diagrams of the S-specimens (left) and L-specimens (right).

The calculation of the effective stiffness of the specimens was based on the method described in section C.3 of EC8-Part 2 [9]. The calculation of the deformation ductility is based on the equations given in Fig. 14 for a cantilever beam. The length of the plastic hinge was calculated as proposed in EC8-Part 2. The results are given in Table 2 considering no gap in the supports for the S-specimens and in Table 3 for the L-specimens.

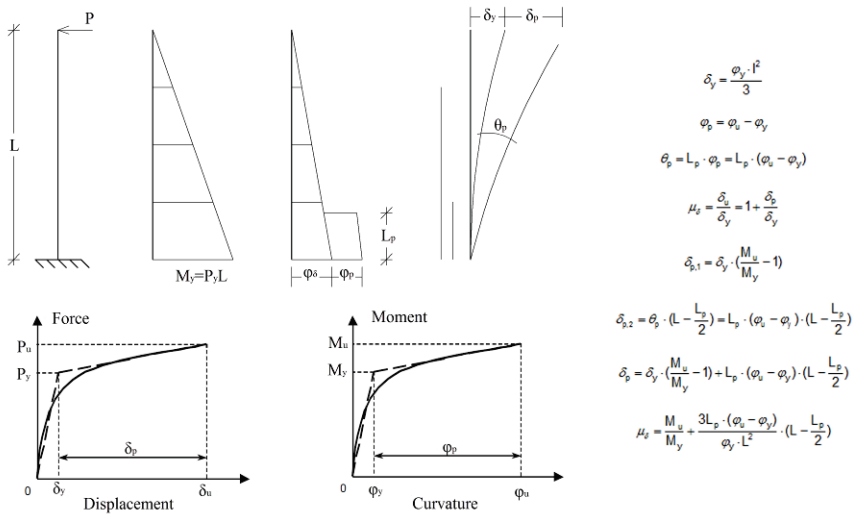

Figure 14: Elastic-plstic behaviour of a cantilever beam.

M_y (kNm)	P_y (kN)	EJ_{eff} / EJ_{un} (%)	φ_y (1/m)	φ_u (1/m)	L_p (mm)	δ_y (mm)	δ_u (mm)	μ_δ
31.25	166.7	33.99	0.033	0.286	114.5	1.5	10.8	6.94

Table 2: Analytical results for the S-specimens.

M_y (kNm)	P_y (kN)	EJ_{eff} / EJ_{un} (%)	φ_y (1/m)	φ_u (1/m)	L_p (mm)	δ_y (mm)	δ_u (mm)	μ_δ
30.85	44.9	35.03	0.034	0.288	225.4	21.2	93.6	4.41

Table 3: Analytical results for the L-specimens.

6 EXPERIMENTAL RESULTS

Interesting results were observed during the experimental procedure regarding the three response indexes, namely, strength, stiffness and ductility. Regarding the L-specimens, flexural cracks were observed in the area around the stiff zone of the beams, which increased along the increase of the imposed deflection and the progressive formation of plastic hinge. Crosswise cracks occurred in S-specimens, which indicated the intense presence of shear effect (Fig. 15). However these specimens managed to deplete their flexural strength as show by the experimental results.

Figure 15: Crack formation in S-4 (left) and L-7 (right).

By processing the specimen hysteresis loops (Fig. 16 and Fig. 17), the results given in Table 4 and Table 5 were obtained. Table 4 summarizes the results considering no gap in the supports while in Table 5 test results are presented by taking into account the existence of the gap. It should be noted that the values of these tables are average values for both directions of cyclic loading. Equation (1) was used for the calculation of the experimental effective stiffness of the cantilevers:

$$P_y \cdot \delta_y = \int_0^L \frac{M^2_{(x)}}{EJ_{eff}} dx + \int_0^L \frac{V^2_{(x)}}{GA_s} dx \quad (1)$$

where $M_{(x)}$ and $V_{(x)}$ are the moment and shear values of the cantilevers, respectively, P_y is the half of the yield load of the beam, δ_y is the yield displacement of the beam, G is the shear modulus considering cracked concrete and A_s is the cantilever section shear area.

	P_y (kN)	δ_y (mm)	δ_u (mm)	EJ_{eff} / EJ_{un} (%)	μ_δ
S-4	172.4	3.4	13.2	13.5	3.91
S-7	174.1	3.6	13.0	12.9	3.61
L-4	44.3	19.9	>93.0	30.8	>4.67
L-7	44.8	20.3	91.5	30.5	4.51

Table 4: Experimental results disregarding the existence of the gap in the supports.

	P_y (kN)	δ_y (mm)	δ_u (mm)	EJ_{eff} / EJ_{un} (%)	μ_δ
S-4	172.4	5.4	15.2	8.5	2.82
S-7	174.1	7.1	16.5	7.1	2.32
L-4	44.3	21.9	>95.0	28.0	>4.36
L-7	44.8	23.8	95	26.0	3.99

Table 5: Experimental results taking into account the existence of the gap in the supports.

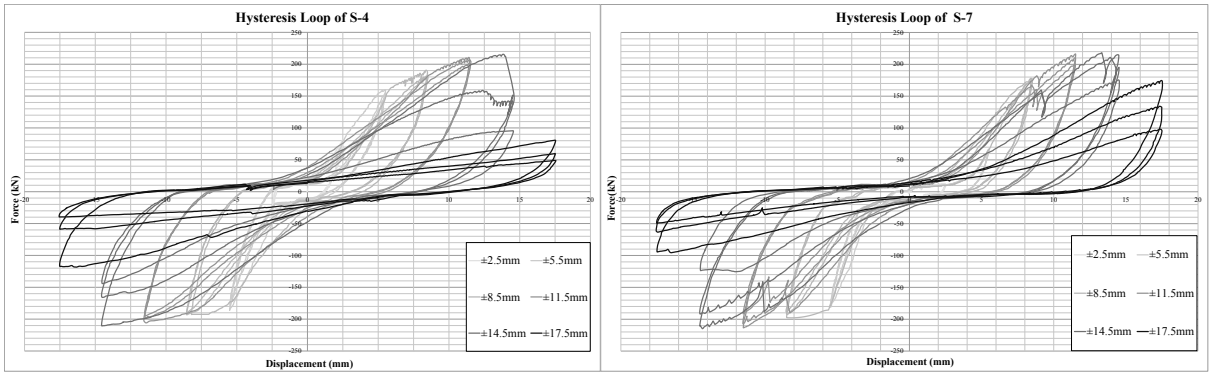

Figure 16: Hysteresis loops of the S-specimens

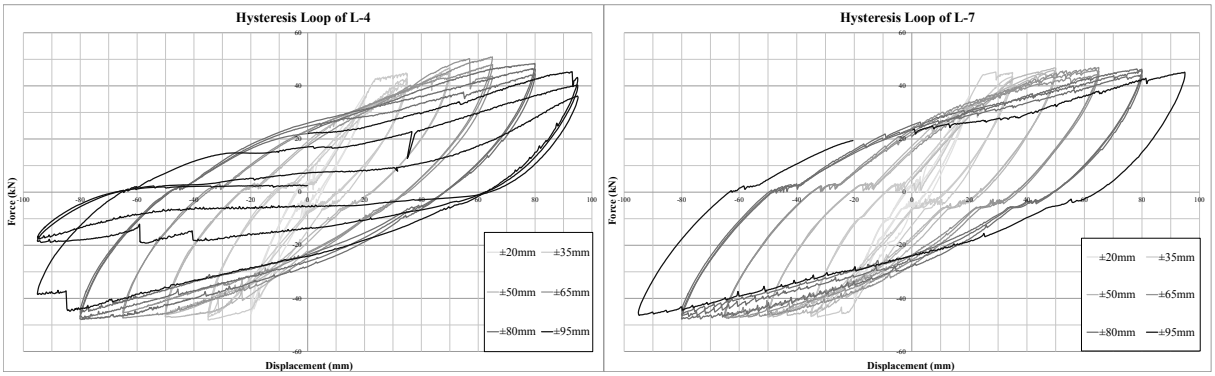

Figure 17: Hysteresis loops of the L-specimens.

By comparing Table 3 to Table 5, regarding the L-specimens, the analytical and experimental results are almost identical. The existence of the gaps at the supports causes no change in the response indexes of the specimens. Regarding the S-specimens and the difference observed between the analytical and experimental results in tables in Table 2 and Table 4 respectively, the following is stated:

- Perhaps the main reason of the results deviation is the non-regularity of these specimens regarding the shear span ratio. In this case the shear span ratio the difference observed between the analytical and experimental results is equal to as=0.375/0.15=2.5 and the shear deformation influences significantly the longitudinal stresses of the specimens.
- Due to the high stiffness of the cantilevers with length of 0.375 m, the consideration of the full fixity of the cantilevers isn't achieved in the side of the rigid zone but inside it near the midlength of the beams.

Regarding the effective stiffness of the L-specimens, where the experimental results can be comparable to the analytical estimation, the experimental values are slightly lower. This is due to the provision of the EC8-Part 2 factor n = 1.20 which is a correction factor representing the effect of the stiffness of the non-cracked part of the cross section. The method presented in the Code concerns the calculation of the effective stiffness at bridge piers where normally the absolute value of the normalized axial force is greater than 0.10, while in this case there was no axial load. The analytical calculation of the effective stiffness omitting the n-factor gives results which are almost identical to the experimental.

Comparing the values of Table 4, it is observed that the existence of gaps in the supports degrades the effective stiffness of the specimens. This effect is more intense in the case of the S-specimens whose yield displacement is comparable to the gap width.

Regarding the available displacement ductility, it is observed that the existence of gaps in the supports affects it meiotically. This decrease is more profound in S-specimens, which are stiffer and have a yield displacement comparable to the gap width. In the case of the L-specimens, whose yield displacement is greater, the effect in the available displacement ductility is minimal. It should be noted that the failure of the specimens was defined as the point at which specimens lose 20% of their strength.

The absolute values of dissipated energy and the dissipated energy per cycle (as a percentage of the dissipated energy of the first cycle of each group of the same displacement level) are presented in Figures 18 to 21. A general increase of the dissipated energy is observed as the deformation increases. The percentage of the dissipated energy of the second and the third cycle compared to the first of each displacement level group increases as the imposed displacements increase and the plastic hinge progressively forms, except of the last two displacement level groups in which the specimens are close to their failure.

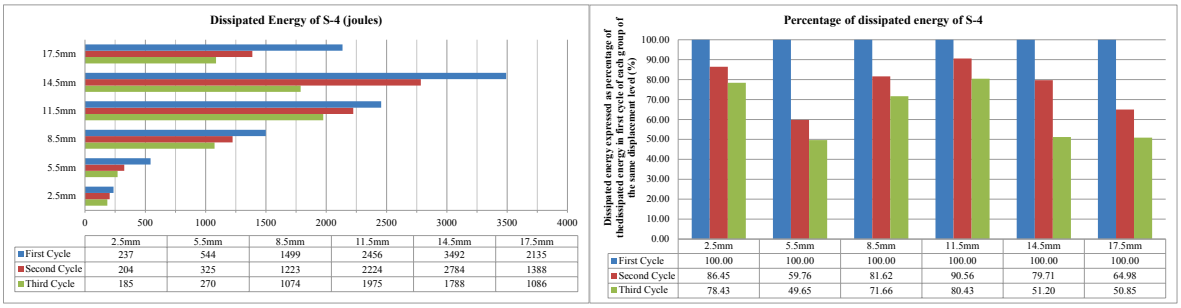

	2.5mm	5.5mm	8.5mm	11.5mm	14.5mm	17.5mm
First Cycle	237	544	1499	2456	3492	2135
Second Cycle	204	325	1223	2224	2784	1388
Third Cycle	185	270	1074	1975	1788	1086

	2.5mm	5.5mm	8.5mm	11.5mm	14.5mm	17.5mm
First Cycle	100.00	100.00	100.00	100.00	100.00	100.00
Second Cycle	86.45	59.76	81.62	90.56	79.71	64.98
Third Cycle	78.43	49.65	71.66	80.43	51.20	50.85

Figure 18: Energy dissipation of specimen S-4.

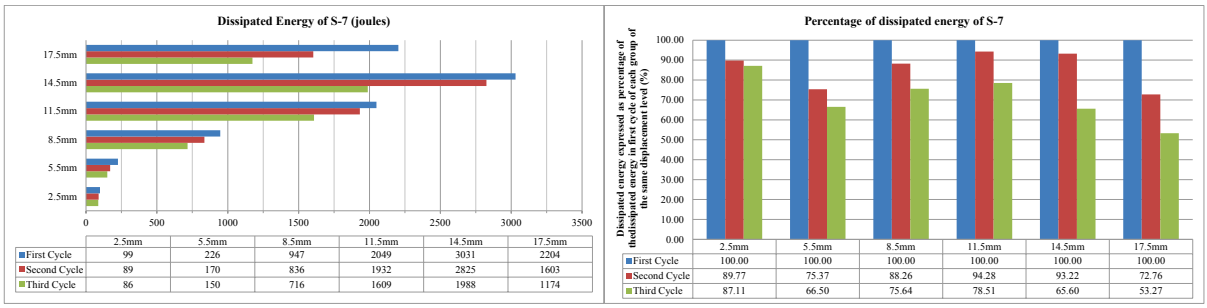

	2.5mm	5.5mm	8.5mm	11.5mm	14.5mm	17.5mm
First Cycle	99	226	947	2049	3031	2204
Second Cycle	89	170	836	1932	2825	1603
Third Cycle	86	150	716	1609	1988	1174

	2.5mm	5.5mm	8.5mm	11.5mm	14.5mm	17.5mm
First Cycle	100.00	100.00	100.00	100.00	100.00	100.00
Second Cycle	89.77	75.37	88.26	94.28	93.22	72.76
Third Cycle	87.11	66.50	75.64	78.51	65.60	53.27

Figure 19: Energy dissipation of specimen S-7.

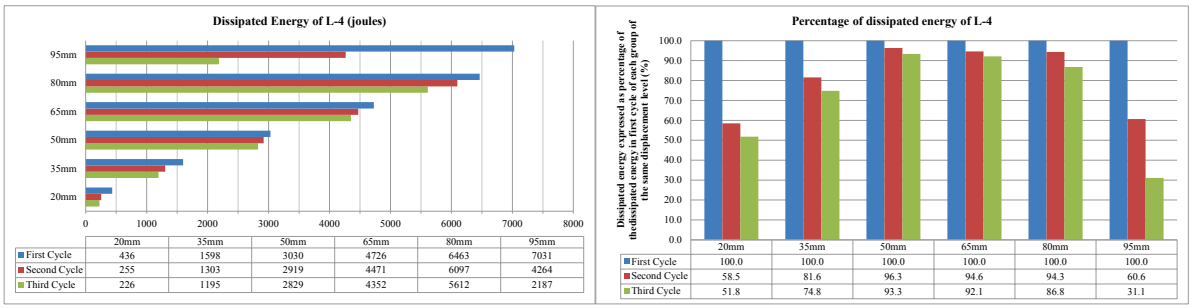

	20mm	35mm	50mm	65mm	80mm	95mm
First Cycle	436	1598	3030	4726	6463	7031
Second Cycle	255	1303	2919	4471	6097	4264
Third Cycle	226	1195	2829	4352	5612	2187

	20mm	35mm	50mm	65mm	80mm	95mm
First Cycle	100.0	100.0	100.0	100.0	100.0	100.0
Second Cycle	58.5	81.6	96.3	94.6	94.3	60.6
Third Cycle	51.8	74.8	93.3	92.1	86.8	31.1

Figure 20: Energy dissipation of specimen L-4.

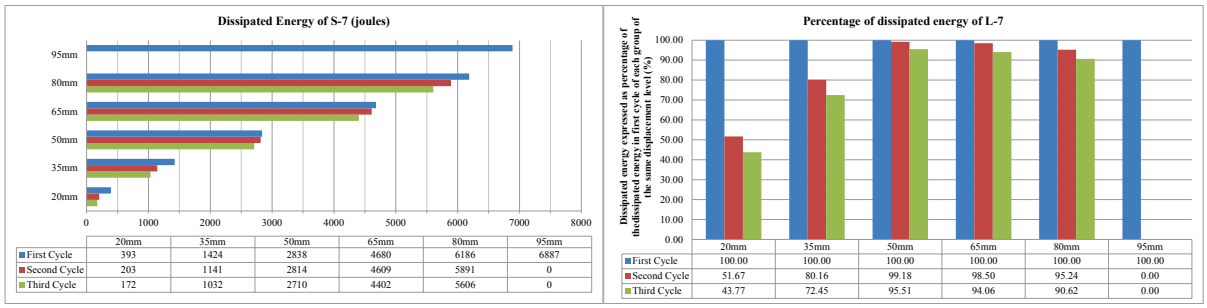

	20mm	35mm	50mm	65mm	80mm	95mm
First Cycle	393	1424	2838	4680	6186	6887
Second Cycle	203	1141	2814	4609	5891	0
Third Cycle	172	1032	2710	4402	5606	0

	20mm	35mm	50mm	65mm	80mm	95mm
First Cycle	100.00	100.00	100.00	100.00	100.00	100.00
Second Cycle	51.67	80.16	99.18	98.50	95.24	0.00
Third Cycle	43.77	72.45	95.51	94.06	90.62	0.00

Figure 21: Energy dissipation of specimen L-7.

The damage factor of the specimens regarding the stiffness loss in each cycle [10] is given in Figures 22 and 23. It is observed that the damage factor is constant and low, around 3 % to 5 %, except of the groups of same displacement level cycles that are near to the failure of the specimens. It is noted that specimen L-7 failed completely during the first cycle of the 95mm imposed displacement.

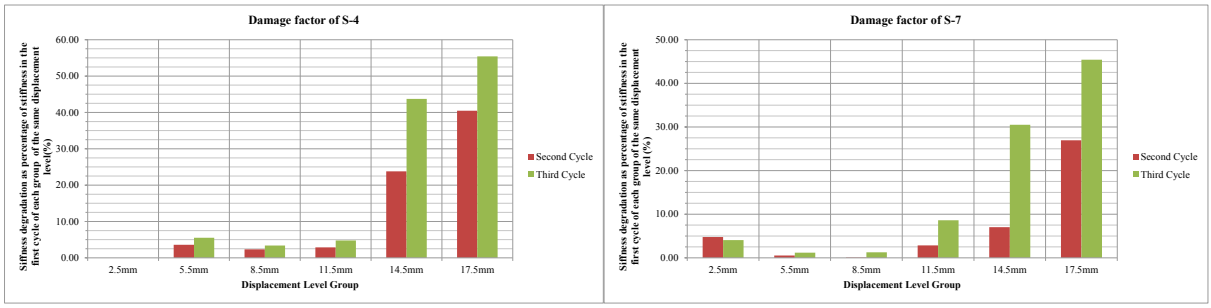

Figure 22: Damage factor (stiffness degradation) of the S-specimens.

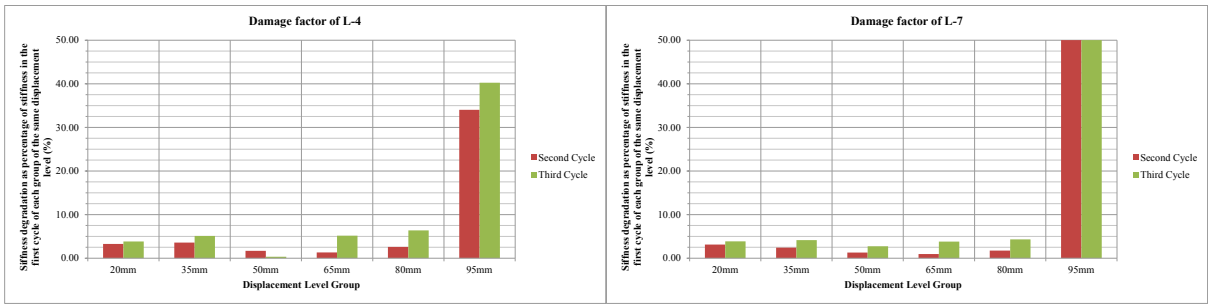

Figure 23: Damage factor (stiffness degradation) of the L-specimens.

7 CONCLUSIONS

The experimental study of the mechanical behavior of a novel mechanism for restraining seismic actions in ductile bridges was presented in this study. In particular, three response indexes were examined namely strength, stiffness and ductility. The importance of the experimental investigation of this mechanism is intensified by the nonlinear behaviour of the mechanism during a seismic event due to the existence of the gap in the support of the abutment wall. Furthermore, the influence of the existence of the gap on energy dissipation capacity and durability of the abutment walls during cyclic loading was examined.

The following conclusions are stated:

- The strength and deformation of the examined specimens with high shear span ratio (long) were similar to the analytically calculated. The same conclusion applies on the available displacement ductility as well. This implies that the existence of the gap in the supports did not affect the mechanical properties of these specimens.
- In the case of specimens with low shear span ratio (short), the analytically calculated strength had no significant difference from the experimentally derived. On the contrary, the experimentally measured specimen deformation and available displacement ductility, disregarding the existence of the gap at the supports, differed from the calculated values. This difference is due to the low shear span ratio of the specimens and their diversion from the pure bending case.
- The existence of the gaps in the supports degrades the specimen stiffness. This decrease is more profound in the stiffer specimens and in the case of wider gaps. This observation confirms the ability of the mechanism to reduce the developing stresses in the serviceability state.

- The gaps in the supports cause the reduction of available displacement ductility. The reduction is higher in the cases of the wider gaps and in stiffer specimens, in which the yield displacement is comparable to the width of the gaps.
- The examined specimens had good behaviour regarding the energy dissipation capacity, regardless of the gap width and shear span ratio. It is observed that in the case of the wider gap, the specimens are activated in higher imposed displacements and this also confirms the ability of the mechanism to reduce the developing stresses in the serviceability state.
- The performance of the examined specimens is considered stable, regardless of the gap width and shear span ratio.

REFERENCES

[1] S. Mitoulis, I. Tegos, *An Unconventional Retraining System for Limiting the Seismic Movements of Isolated Bridges.* Engineering Structures, Elsevier Ltd., **32**: 1100-1112, 2010.

[2] V. Pilitsis, M. Skordeli, I. Tegos, A Suggestion for Adjustment of the Load-Bearing Structure of Bridges with Antiseismic, Economic and Aesthetic Benefits. *2013 FIB International Symposium,* Tel-Aviv, Israel, April 22-24, 2013.

[3] V. Piltisis, I. Tegos, Employment of Abutments and Approach Embankments for Seismic Protection of Bridges. *2013 International Van Earthquake Symposium,* Van, Turkey, October 23-27, 2013.

[4] D. Anastasopoulos, Z. Kopelia, V. Piltisis, I Tegos, Conventional and Alternative Design of Highway Bridge in Egnatia Motorway Including many Innovative Solutions. *International Conference IBSBI 2014, "Innovations on Bridges and Soil-Bridge Interaction",* Athens, Greece, October 16-18, 2014.

[5] CEN [Comité Européen de Normalisation], EN 1992-1-1: Eurocode 2: Design of Concrete Structures - Part 1-1: General Rules and Rules for Buildings, 2004.

[6] K.-A. Stylianidis, K.V. Papanikolaou, C. Ignatakis, T. Salonikios, The Novel Cycle-Loading System of The Laboratory of Reinforced Concrete and Masonry of A.U.Th. - Potential and First Applications (Greek). *11th Greek Conference on Reinforced Concrete,* Corfu, Greece, May 18-20, 1994.

[7] V. K. Papanikolaou, *Analysis of arbitrary composite sections in biaxial bending and axial load.* Computers & Structures **98-99**, 33-54, 2012.

[8] R. Park, R.A. Sampson, *Ductility of Reinforced Concrete Column Sections in Seismic Design,* Journal of the ACI, **69-9**: 543-551, 1972.

[9] CEN [Comité Européen de Normalisation], EN 1998-2: Eurocode 8: Design of Structures for Earthquake Resistance - Part 2: Bridges, 2005.

[10] S.K. Kunnath, C. Jenne, Seismic Damage Assessment of Inelastic RC Structures, *5th U.S. National Conference on Earthquake Engineering*, Chicago, U.S.A., July 10-14, 1994.